

Exclusive $B \rightarrow V\gamma$ decays in the T2HDM

Zhenjun Xiao,^{*} Huihui Cheng, and Linxia Lü[†]

*Department of Physics and Institute of Theoretical Physics,
Nanjing Normal University, Nanjing, Jiangsu 210097, P.R.China*

(Dated: November 2, 2018)

Abstract

By employing the QCD factorization approach for the exclusive $B \rightarrow V\gamma$ decays, we calculated the new physics contributions to the branching ratios, CP asymmetries, isospin and U-spin symmetry breaking of $B \rightarrow K^*\gamma$ and $B \rightarrow \rho\gamma$ decays, induced by the charged Higgs penguin diagrams appeared in the top-quark two-Higgs-doublet model(T2HDM). Within the considered parameter space, we found that (a) a charged-Higgs boson with a mass larger than 300 GeV are always allowed by the date of $B \rightarrow V\gamma$ decay, and such lower limit on M_H are comparable with those obtained from the inclusive $B \rightarrow X_s\gamma$ decay; (b) the CP asymmetry of $B \rightarrow \rho\gamma$ in the T2HDM can be as large as 10% in magnitude and has a strong dependence on the angle θ and the CKM angle γ ; (c) the isospin symmetry breakings of $B \rightarrow V\gamma$ decays in the T2HDM are generally small in size: around 6% for $B \rightarrow K^*\gamma$ decay and less than 20% for $B \rightarrow \rho\gamma$ decay; and (d) the U-spin symmetry breaking $\Delta U(K^*, \rho)$ in the T2HDM is also small in size, only about 8% of the branching ratio $\mathcal{B}(B \rightarrow \rho^0\gamma)$.

PACS numbers: 13.20.He, 12.60.Fr, 14.40.Nd

arXiv:hep-ph/0512359v1 29 Dec 2005

^{*}Electronic address: xiaozhenjun@njnu.edu.cn

[†]Electronic address: lulinxia@email.njnu.edu.cn

I. INTRODUCTION

As is well known, the inclusive radiative decays $B \rightarrow X_q \gamma$ with $q = (d, s)$ and the corresponding exclusive decays $B \rightarrow V \gamma$ ($V = K^*, \rho, \omega$) are very sensitive to the flavor structure of the standard model (SM) and to the new physics models beyond the SM [1, 2, 3].

For the inclusive $B \rightarrow X_s \gamma$ decay, the world average of the experimental measurements [4] is

$$\mathcal{B}(B \rightarrow X_s \gamma)^{exp} = (3.39_{-0.27}^{+0.30}) \times 10^{-4}, \quad (1)$$

which agrees very well with the next-to-leading order (NLO) SM prediction [3, 5]. The perfect agreement leads to strong constraints on many new physics models [3, 6, 7, 8, 9] where new particles, such as the charged Higgs boson, charginos and /or gluinos, may provide significant contributions to the studied radiative process through flavor changing loop (box or penguin) diagrams.

The exclusive decay mode $B \rightarrow K^* \gamma$ has a very clean experimental signal and a low background, and have been measured with high accuracy. The world averages of the CP-averaged branching ratios as given by Heavy Flavor Averaging Group (HFAG) are [4]

$$\begin{aligned} \mathcal{B}(B^0 \rightarrow \overline{K}^{*0} \gamma) &= (40.1 \pm 2.0) \times 10^{-6}, \\ \mathcal{B}(B^\pm \rightarrow K^{*\pm} \gamma) &= (40.3 \pm 2.6) \times 10^{-6}. \end{aligned} \quad (2)$$

The Cabibbo-suppressed $b \rightarrow d \gamma$ decay and the corresponding exclusive $B \rightarrow (\rho, \omega) \gamma$ decays were also measured very recently [4, 10]

$$\begin{aligned} \mathcal{B}(B \rightarrow \rho^+ \gamma) &= (0.68_{-0.31}^{+0.36}) \times 10^{-6}, \\ \mathcal{B}(B \rightarrow \rho^0 \gamma) &= (0.38 \pm 0.18) \times 10^{-6}, \\ \mathcal{B}(B \rightarrow \rho \gamma) &= (0.96 \pm 0.23) \times 10^{-6}, \\ \mathcal{B}(B \rightarrow \omega \gamma) &= (0.54_{-0.21}^{+0.23}) \times 10^{-6}. \end{aligned} \quad (3)$$

$$\mathcal{B}(B \rightarrow \omega \gamma) = (0.54_{-0.21}^{+0.23}) \times 10^{-6}. \quad (4)$$

Measurements of these exclusive branching fractions would improve the constraint on the ratio $|V_{td}/V_{ts}|$ in the context of the SM, and provide sensitivity to new physics beyond the SM that is complementary to those from $b \rightarrow s \gamma$ and $B \rightarrow K^* \gamma$ decays.

When compared with the inclusive $b \rightarrow (s, d) \gamma$ decays, the corresponding exclusive $B \rightarrow V \gamma$ decays are experimentally more tractable but theoretically less clean, since the bound state effects are essential and need to be described by some non-perturbative quantities like form factors and light-cone distribution amplitudes (LCDAs).

In the framework of the SM, the $B \rightarrow V \gamma$ decays have been investigated in leading or next-to-leading order by employing the constituent quark model (CQM)[11, 12]. The exclusive $B \rightarrow (K^*, \rho) \gamma$ decays have been studied by using a QCD factorization approach [13, 14, 15, 16, 17], or by employing the perturbative QCD (pQCD) approach [18, 19]. Such exclusive decay modes have also been studied recently in some new physics models beyond the SM [20, 21].

In this paper, we calculate the new physics contributions to the branching ratios, CP asymmetries, the isospin and U-spin symmetry breaking of the exclusive radiative decays $B \rightarrow (K^*, \rho) \gamma$ in the framework of the top-quark two-Higgs-doublet model (T2HDM)

[22, 23, 24]. The QCD factorization method for exclusive $B \rightarrow V\gamma$ decays as presented in Refs.[13, 14, 15] will be employed in our calculations.

This paper is organized as follows. In Sec. II, we present the relevant formulas for the calculation of Wilson coefficients, the branching ratio $\mathcal{B}(B \rightarrow X_s\gamma)$ and some physical observables in the SM and T2HDM. In Sec. III and IV, we calculate the new physics contributions to the $B \rightarrow K^*\gamma$ and $B \rightarrow \rho\gamma$ decay in T2HDM, respectively. The conclusions are included in the final section.

II. THEORETICAL FRAMEWORK

For the standard model part, we follow the procedure of Ref. [15] and use the formulas as presented in Refs.[15, 16]. The QCD factorization approach to the exclusive $B \rightarrow V\gamma$ decays was applied independently in Refs.[13, 14, 15] with some differences in the definition and explicit expressions of functions. We adopt the analytical formulas in the SM as presented in Refs.[15, 16] in this paper, since more details can be found there.

A. Effective Hamiltonian for $b \rightarrow s\gamma$

In the framework of the SM, if we only take into account operators up to dimension 6 and put $m_s = 0$, the effective Hamiltonian for $b \rightarrow s\gamma$ transitions at the scale $\mu \approx m_b$ reads [15]

$$\mathcal{H}_{eff} = \frac{G_F}{\sqrt{2}} \sum_{p=u,c} \lambda_p^s \left[C_1 Q_1^p + C_2 Q_2^p + \sum_{j=3}^8 C_j Q_j \right] \quad (5)$$

where $\lambda_p^q = V_{pq}^* V_{pb}$ for $q = (d, s)$ is the Cabibbo-Kobayashi-Maskawa (CKM) factor [25]. And the current-current, QCD penguin, electromagnetic and chromomagnetic dipole op-

erators in the standard basis ¹ are given by

$$\begin{aligned}
Q_1^p &= (\bar{s}p)_{V-A}(\bar{p}b)_{V-A}, \\
Q_2^p &= (\bar{s}_\alpha p_\beta)_{V-A}(\bar{p}_\beta b_\alpha)_{V-A}, \\
Q_3 &= (\bar{s}b)_{V-A} \sum (\bar{q}q)_{V-A}, \\
Q_4 &= (\bar{s}_\alpha b_\beta)_{V-A} \sum (\bar{q}_\beta q_\alpha)_{V-A}, \\
Q_5 &= (\bar{s}b)_{V-A} \sum (\bar{q}q)_{V+A}, \\
Q_6 &= (\bar{s}_\alpha b_\beta)_{V-A} \sum (\bar{q}_\beta q_\alpha)_{V+A}, \\
Q_7 &= \frac{e}{8\pi^2} m_b \bar{s}_\alpha \sigma^{\mu\nu} (1 + \gamma_5) b_\alpha F_{\mu\nu}, \\
Q_8 &= \frac{g}{8\pi^2} m_b \bar{s}_\alpha \sigma^{\mu\nu} (1 + \gamma_5) T_{\alpha\beta}^a b_\beta G_{\mu\nu}^a,
\end{aligned} \tag{6}$$

where T_a ($a = 1, \dots, 8$) stands for $SU(3)_c$ generators, α and β are color indices, e and g_s are the electromagnetic and strong coupling constants, Q_1 and Q_2 are current-current operators, $Q_3 - Q_6$ are the QCD penguin operators, Q_7 and Q_8 are the electromagnetic and chromomagnetic penguin operators. The effective Hamiltonian for $b \rightarrow d\gamma$ is obtained from Eqs.(5) - (6) by the replacement $s \rightarrow d$.

To calculate the exclusive $B \rightarrow V\gamma$ decays complete to next-to-leading order in QCD and to leading order in Λ_{QCD}/M_B , only the NLO Wilson coefficient $C_7(\mu_b)$ and LO Wilson coefficients $C_i(\mu_b)$ with $i = (1 - 6, 8)$ and $\mu_b = \mathcal{O}(m_b)$ are needed. For the sake of the readers, we simply present these Wilson coefficients at the scale $\mu_W = M_W$ and $\mu_b = m_b$ in Appendix A.

In literature, one usually uses certain linear combinations of the original $C_i(\mu)$, the so-called ‘‘effective coefficients’’ $C_i^{\text{eff}}(\mu)$ introduced in Refs.[26, 27], in ones calculation. The corresponding transformations are of the form

$$C_i^{\text{eff}}(\mu) = C_i(\mu), \quad (i = 1, \dots, 6), \tag{7}$$

$$C_7^{\text{eff}}(\mu) = C_7(\mu) + \sum_{i=1}^6 y_i C_i(\mu), \tag{8}$$

$$C_8^{\text{eff}}(\mu) = C_8(\mu) + \sum_{i=1}^6 z_i C_i(\mu), \tag{9}$$

with $\vec{y} = (0, 0, 0, 0, -1/3, -1)$ and $\vec{z} = (0, 0, 0, 0, 1, 0)$ in the NDR scheme [27], and $\vec{y} = (0, 0, -1/3, -4/9, -20/3, -80/9)$ and $\vec{z} = (0, 0, 1, 1/6, 20, -10/3)$ in the \overline{MS} scheme with fully anticommuting γ_5 [26]. In order to simplify the notation we will also omit the label ‘‘eff’’ throughout this paper.

¹ There is another basis: the CMM basis, introduced by Chetyrkin, Misiak, and Münz [26] where the fully anticommuting γ_5 in dimensional regularization are employed. The corresponding operators and Wilson coefficients in the CMM basis are denoted as P_i and Z_i in [15]. For the numbering of operators $Q_{1,2}^p$, we use the same convention as Ref. [16] throughout this paper.

B. $B \rightarrow V\gamma$ decay in the SM

Based on the effective Hamiltonian for the quark level process $b \rightarrow s(d)\gamma$, one can write down the amplitude for $B \rightarrow V\gamma$ and calculate the (CP-averaged) branching ratios and CP violating asymmetries once a method is derived for computing the hadronic matrix elements. By using the QCD factorization approach [13, 14, 15], one can separate systematically perturbatively calculable hard scattering kernels (T_i^I and T_i^{II}) from nonperturbative form factors and universal light-cone distribution amplitudes of B , K^* and ρ mesons. The higher order QCD corrections can therefore be taken into account consistently.

In QCD factorization approach, the hadronic matrix elements of the operators Q_i with $i = 1, \dots, 8$ for $B \rightarrow V\gamma$ decays can be written as [15]

$$\langle V\gamma(\epsilon)|Q_i|\bar{B}\rangle = \left[F^{B \rightarrow V}(0) T_i^I + \int_0^1 d\xi dv T_i^{II}(\xi, v) \Phi_B(\xi) \Phi_V(v) \right] \cdot \epsilon \quad (10)$$

where ϵ is the photon polarization 4-vector, $F^{B \rightarrow V}$ is the form factor describing $B \rightarrow V$ decays, Φ_B and Φ_V are the universal and nonperturbative light-cone distribution amplitudes for B and V meson respectively², v ($\bar{v} \equiv 1 - v$) is the momentum fraction of a quark (anti-quark) inside a light meson: $l_1^+ = vk^+$ and $l_2^+ = \bar{v}k^+$ while $k^\mu = (k^+, k^-, \vec{k}_\perp)$ is a four vector in the light-cone coordinator, ξ describes the momentum fraction of the light spectator quark inside a B meson: $l^+ = \xi p_B^+$ with $\xi = \mathcal{O}(\Lambda_{QCD}/m_b)$, and T_i^I and T_i^{II} denote the perturbative short-distance interactions. The QCD factorization formula (10) holds up to corrections of relative order Λ_{QCD}/m_b .

In the heavy quark limit, the contributions to the exclusive $B \rightarrow V\gamma$ decay can be classified into three classes [16]: (a) the ‘‘hard vertex’’ contributions, (b) the ‘‘hard spectator’’ contributions and (c) the ‘‘Weak annihilation’’ contribution. Combining these three parts together, the decay amplitude to $\mathcal{O}(\alpha_s)$ for exclusive $B \rightarrow V\gamma$ decay takes the form of

$$A(\bar{B} \rightarrow V\gamma) = \frac{G_F}{\sqrt{2}} R_V \langle V\gamma|Q_7|\bar{B}\rangle, \quad (11)$$

with

$$R_V = \lambda_u^{(q)} [a_7^u(V\gamma) + a_{ann}^u(V\gamma)] + \lambda_c^{(q)} [a_7^c(V\gamma) + a_{ann}^c(V\gamma)], \quad (12)$$

where $q = s$ for $V = K^*$, $q = d$ for $V = \rho$, and a_7^p ($p = u, c$) denote the hard vertex and hard spectator NLO contributions

$$a_7^p(V\gamma) = C_7^0(\mu) + \frac{\alpha_s(\mu)C_F}{4\pi} \left[\sum_{i=1,2} Z_i^0(\mu)G_i(z_p) + \sum_{j=3\dots 6,8} Z_j^0(\mu)G_j \right] + \frac{\alpha_s(\mu_h)C_F}{4\pi} \left[C_1^0(\mu_h)H_1^V(z_p) + \sum_{j=3\dots 6,8} C_j^0(\mu_h)H_j^V \right], \quad (13)$$

² For explicit expressions and more details about Φ_B and Φ_V , one can see Ref. [13] and references therein.

where $z_q = m_q^2/m_b^2$, $\mu_h = \sqrt{0.5\mu}$, $C_F = 4/3$, $Z_j^0(\mu)$ for $j = 1 \dots 8$ are the Wilson coefficients defined in the CMM basis [26]. The explicit expressions of the Wilson coefficients and the functions G_i and H_j^V can be found in Ref. [16] and in Appendix A and B. The functions a_{ann}^u and a_{ann}^c in Eq. (12) denote the weak annihilation contributions and can be found in Ref. [16].

One special feature of the $B \rightarrow \rho\gamma$ decay is that the weak annihilation can proceed through the current-current operator with large Wilson coefficient C_1 . Although the annihilation contribution is power-suppressed in $1/m_b$, but it is compensated by the large Wilson coefficient and the occurrence of annihilation at tree level.

From the decay amplitude in Eq. (11), it is straightforward to write down the branching ratio for $\overline{B} \rightarrow V\gamma$ decay

$$\mathcal{B}(\overline{B} \rightarrow V\gamma) = \tau_B \frac{G_F^2 \alpha m_B^3 m_b^2}{32\pi^4} \left(1 - \frac{m_V^2}{m_B^2}\right)^3 |R_V|^2 c_V^2 |F_V|^2, \quad (14)$$

where function R_V has been given in Eq. (12), and $c_V = 1$ for $V = K^*, \rho^-$ and $c_V = 1/\sqrt{2}$ for $V = \rho^0$. The branching ratios for the CP-conjugated $B \rightarrow V\gamma$ decay are obtained by the replacement of $\lambda_p^{(q)} \rightarrow \lambda_p^{(q)*}$ in function R_V .

C. Outline of the T2HDM

Among all the three generation leptons and quarks discovered so far, the top quark is the unique one: which is much heavier than all other fermions. Since its discovery in 1995, many efforts have been made to explain its large mass by considering the specific Yukawa couplings appeared in the physics models beyond the SM, the T2HDM [22, 23, 24] is one of such kind of new physics models.

The T2HDM is in fact a special case of the third type of two-Higgs-doublet model, the model III [28, 29, 30]. In T2HDM, the top quark is the only fermion receiving its large mass from the vacuum expectation value (VEV) of the second Higgs doublet ϕ_2 , $\langle \phi_2 \rangle_{vac} = v_2/\sqrt{2}$ is large. Other five quarks receive their masses from the VEV of the first Higgs doublet ϕ_1 , whose VEV $\langle \phi_1 \rangle_{vac} = v_1/\sqrt{2}$ is much smaller. Furthermore, a new source of CP violation is appeared here: the charged Higgs sector of the model contains a CP-violating phase “ θ ” ($\xi = |\xi|e^{-i\theta}$) in addition to the usual Cabibbo-Kobayashi-Maskawa (CKM) phase δ of the SM.

The lagrangian density of Yukawa interactions of the T2HDM can be simply written as follows [23, 24]:

$$\mathcal{L}_Y = -\bar{L}_L \phi_1 E l_R - \bar{Q}_L \phi_1 F d_R - \bar{Q}_L \tilde{\phi}_1 G \mathbf{1}^{(1)} u_R - \bar{Q}_L \tilde{\phi}_2 G \mathbf{1}^{(2)} u_R + H.C., \quad (15)$$

where the two Higgs doublets are denoted by ϕ_i with $\tilde{\phi}_i = i\sigma^2 \phi_i^*$ ($i = 1, 2$), and where E, F, G are 3×3 matrices in generation space; $\mathbf{1}^{(1)} \equiv \text{diag}(1, 1, 0)$, and $\mathbf{1}^{(2)} \equiv \text{diag}(0, 0, 1)$ are two orthogonal projection operators onto the first two and the third family respectively, and Q_L and L_L are the usual left-handed quark and lepton doublets, while l_R, u_R and d_R are the right-handed singlets. The heaviness of the top quark arises as a result of the much large VEV of ϕ_2 to which no other quark couples. For this reason, we set that $\tan\beta = v_2/v_1 \geq 10$ throughout this paper.

The Yukawa couplings induced by the charged Higgs penguins can be written as [23, 24]

$$\begin{aligned} \mathcal{L}_Y^C = & \frac{g}{\sqrt{2}M_W} \left\{ -\bar{u}_L V M_D d_R [G^+ - \tan\beta H^+] + \bar{u}_R M_U V d_L [G^+ - \tan\beta H^+] \right. \\ & \left. + \bar{u}_R \Sigma^+ V d_L [\tan\beta + \cot\beta] H^+ + H.C. \right\} \end{aligned} \quad (16)$$

where G^\pm represent the would-be Goldstone bosons, $M_U = \text{diag}(m_u, m_c, m_t)$ and $M_D = \text{diag}(m_d, m_s, m_b)$ are the diagonal mass matrices for up- and down-type quarks respectively, V is the usual CKM matrix and $\Sigma \equiv M_U U_R^+ \mathbf{1}^{(2)} U_R$, and the U_R^+ is the unitary matrix which diagonalizes the right handed up-type quarks.

As defined in Ref. [23], the matrix Σ can be written as

$$\Sigma \equiv M_U U_R^+ \mathbf{1}^{(2)} U_R = \begin{pmatrix} 0 & 0 & 0 \\ 0 & m_c \epsilon_{ct}^2 |\xi|^2 & m_c \epsilon_{ct} \xi^* \sqrt{1 - |\epsilon_{ct} \xi|^2} \\ 0 & m_c \xi^* \sqrt{1 - |\epsilon_{ct} \xi|^2} & m_t (1 - |\epsilon_{ct} \xi|^2) \end{pmatrix} \quad (17)$$

where $\epsilon_{ct} \equiv m_c/m_t$, $\xi = |\xi|e^{-i\theta}$ is a complex number of order unity. In the framework of the T2HDM, many studies have been done [22, 23, 24]. In this paper, based on previous works and currently available precision data, we focus on the calculation of the new physics contributions to the exclusive $B \rightarrow V\gamma$ decays induced by the charge-Higgs penguin diagrams.

D. Wilson coefficients C_7^0 and C_8^0 in the T2HDM

The new physics contributions to the quark level $b \rightarrow (s, d)\gamma$ transition from the charged Higgs penguins manifest themselves from the correction to the Wilson coefficients at the matching scale M_W .

For the exclusive decays $B \rightarrow V\gamma$ and to the first order in α_s , only the NLO expression for $C_7(\mu)$ has to be used while the leading order values are sufficient for other Wilson coefficients appeared in $a_7^p(V\gamma)$ in Eq. (13). For the SM part, the required Wilson coefficients can be found in Appendix A. For the T2HDM part, only the leading order C_7^{NP} and C_8^{NP} are known at present [23, 24] and will be taken into account in our studies for the exclusive $B \rightarrow V\gamma$ decays.

The leading order Wilson coefficients C_7^{NP} and C_8^{NP} at the matching scale M_W take the form [23, 24],

$$\begin{aligned} C_7^{\text{NP}}(M_W) = & \sum_{i=c,t} k^{iq} \left[-\tan^2\beta + \frac{1}{m_i V_{iq}^*} (\Sigma^T V^*)_{iq} \times (\tan^2\beta + 1) \right] \left\{ B(y_i) + \frac{1}{6} A(y_i) \times \right. \\ & \left. \left[-1 + \frac{1}{m_i V_{ib}} (\Sigma^+ V)_{ib} (\cot^2\beta + 1) \right] \right\}, \end{aligned} \quad (18)$$

$$\begin{aligned} C_8^{\text{NP}}(M_W) = & \sum_{i=c,t} k^{iq} \left[-\tan^2\beta + \frac{1}{m_i V_{iq}^*} (\Sigma^T V^*)_{iq} \times (\tan^2\beta + 1) \right] \left\{ E(y_i) + \frac{1}{6} D(y_i) \times \right. \\ & \left. \left[-1 + \frac{1}{m_i V_{ib}} (\Sigma^+ V)_{ib} (\cot^2\beta + 1) \right] \right\}, \end{aligned} \quad (19)$$

where $k^{iq} = -V_{ib}V_{iq}^*/(V_{tb}V_{tq}^*)$, $y_i = (m_i/m_H)^2$, V denotes the CKM matrix, and the matrix Σ is defined in Eq. (17). The functions A , B , D and E in Eqs.(18) and (19) are of the form

$$A(x) = \frac{-7x + 5x^2 + 8x^3}{24(1-x)^3} - \frac{2x^2 - 3x^3}{4(1-x)^4} \log[x], \quad (20)$$

$$B(x) = \frac{3x - 5x^2}{12(1-x)^2} + \frac{2x - 3x^2}{6(1-x)^3} \log[x], \quad (21)$$

$$D(x) = \frac{-2x - 5x^2 + x^3}{8(1-x)^3} - \frac{3x^2}{4(1-x)^4} \log[x], \quad (22)$$

$$E(x) = \frac{3x - x^2}{4(1-x)^2} + \frac{x}{2(1-x)^3} \log[x]. \quad (23)$$

At low energy scale $\mu = \mathcal{O}(m_b)$, the leading order Wilson coefficients $C_7^0(\mu)$ and $C_8^0(\mu)$ after the inclusion of new physics contributions can be written as

$$\begin{aligned} C_7^0(\mu) &= \eta^{\frac{16}{23}} [C_{7,\text{SM}}^0(M_W) + C_7^{\text{NP}}(M_W)] \\ &+ \frac{8}{3} \left(\eta^{\frac{14}{23}} - \eta^{\frac{16}{23}} \right) [C_{8,\text{SM}}^0(M_W) + C_8^{\text{NP}}(M_W)] + \sum_{i=1}^8 h_i \eta^{a_i}, \end{aligned} \quad (24)$$

$$C_8^0(\mu) = \eta^{\frac{14}{23}} [C_{8,\text{SM}}^0(M_W) + C_8^{\text{NP}}(M_W)] + \sum_{i=1}^8 \tilde{h}_i \eta^{a_i}, \quad (25)$$

where $\eta = \alpha_s(M_W)/\alpha_s(\mu_b)$, and the ‘‘magic numbers’’ h_i , \tilde{h}_i and a_i can be found in Ref. [1].

E. branching ratio $\mathcal{B}(B \rightarrow X_s \gamma)$

In Refs.[22, 23, 24], the authors have calculated, for example, the new physics corrections to the electric dipole moment(EDM) of the electron, $F^0 - \bar{F}^0$ mixing ($F = K^0, D^0$), $B \rightarrow J/\psi K_S$ decay, and the branching ratios and CP-violating asymmetries of $b \rightarrow (s, d)\gamma$ decays. Some interesting predictions were found, and the constraints on the parameter space of the T2HDM were also obtained by comparing the T2HDM predictions with the data available at that time [22, 23, 24].

The branching ratio of $B \rightarrow X_s \gamma$ at the NLO level can be written as

$$\mathcal{B}(B \rightarrow X_s \gamma)_{NLO} = \mathcal{B}_{SL} \left| \frac{V_{ts}^* V_{tb}}{V_{cb}} \right|^2 \frac{6\alpha_{em}}{\pi f(z)k(z)} [|\bar{D}|^2 + A + \Delta], \quad (26)$$

where $\mathcal{B}_{SL} = (10.64 \pm 0.23)\%$ is the measured semileptonic branching ratio of B meson. $\alpha_{em} = 1/137.036$ is the fine-structure constant, $z = m_c^{pole}/m_b^{pole} = 0.29 \pm 0.02$ is the ratio of the quark pole mass, where $m_b^{pole} = 4.8 \text{ GeV}$. The function $f(z)$ and $k(z)$ denote the phase space factor and the QCD correction for the semileptonic B decay [31]. The term \bar{D} in Eq. (26) corresponds to the subprocess $b \rightarrow s \gamma$

$$\bar{D} = C_7(\mu_b) + V(\mu_b). \quad (27)$$

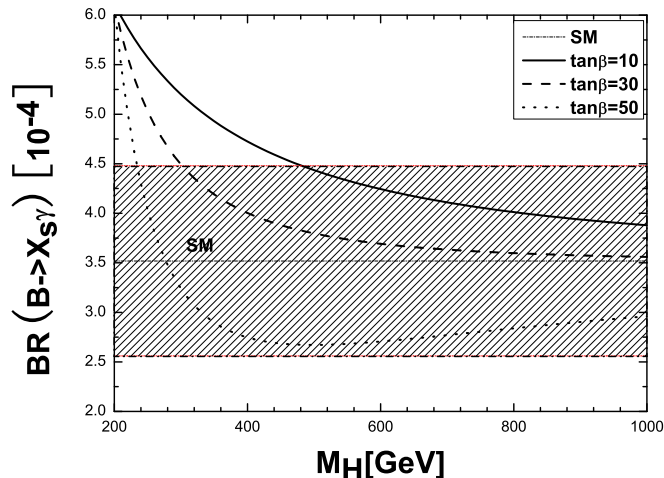


FIG. 1: The M_H dependence of branching ratio $\mathcal{B}(B \rightarrow X_s \gamma)$ in the T2HDM. The gray band shows the data at 3σ level. The dot-dashed line refers to the SM prediction, while the solid, dashed and dots curves show the T2HDM predictions for $\tan \beta = 10, 30$ and 50 , respectively.

The explicit expressions of the function $V(\mu_b)$, A and Δ can be found easily in Ref. [31]. The term A is the correction coming from the bremsstrahlung process $b \rightarrow s\gamma g$, while the term Δ includes the non-perturbative $1/m_b$ and $1/m_c$ corrections. The numerical results show that the new physics contributions to “small quantities” $A(\mu_b)$ and $\Delta(\mu_b)$ are very small in magnitude and can be neglected safely.

Using Eq. (26) and the input parameters as given in Table I, it is easy to calculate the branching ratio $\mathcal{B}(B \rightarrow X_s \gamma)$. The numerical result is

$$\mathcal{B}(B \rightarrow X_s \gamma)_{NLO}^{SM} = (3.52 \pm 0.32) \times 10^{-4}, \quad (28)$$

in the SM, and

$$\mathcal{B}(B \rightarrow X_s \gamma)^{T2HDM} = (4.00 \pm 0.35) \times 10^{-4} \quad (29)$$

for fixed $M_H = 400$ GeV, $\xi = 1$ and $\tan \beta = 30$, here the major errors from different sources have been added in quadrature.

In Fig. 1, we show the M_H dependence of the branching ratio in T2HDM directly. The dot-dashed line shows the central value of the SM prediction, while the solid, dashed and dots curves show the T2HDM prediction for $\tan \beta = 10, 30$ and 50 , respectively. One can also read out the lower limits on M_H from Fig. 1 directly, for example,

$$330 \text{ GeV} \leq M_H, \quad \text{for } \tan \beta = 30. \quad (30)$$

Of course, the lower limit on the mass M_H has a strong $\tan \beta$ dependence.

III. $B \rightarrow K^* \gamma$ DECAY

Now we are ready to calculate the numerical results for the $B \rightarrow V \gamma$ decay in the T2HDM. For the numerical calculations, unless otherwise specified, we use the central values of the input parameters as listed in Table I, and consider the uncertainties of those parameters as given explicitly in Table I.

TABLE I: Values of the input parameters used in the numerical calculations [32, 33, 34]. For the value of F_{K^*} , we use the lattice QCD determination of $F_{K^*} = 0.25 \pm 0.06$ [34] instead of the result $F_{K^*} = 0.38 \pm 0.06$ as given in Ref. [33]. The smaller value of F_{K^*} gives a better agreement between the SM predictions and the data. The definition of the Wolfenstein parameter R_b is $R_b = \sqrt{\bar{\rho}^2 + \bar{\eta}^2}$.

A	λ	R_b	γ	G_F	α_{em}
0.854	0.2200	0.39 ± 0.06	$(60 \pm 14)^\circ$	$1.1664 \times 10^{-5} GeV^{-2}$	1/137.036
$\alpha_s(M_Z)$	m_W	m_t	$\Lambda_{\overline{MS}}^{(5)}$	$m_c(m_b)$	m_u
0.119	80.42 GeV	174.3 GeV	225 MeV	1.3 ± 0.2 GeV	4.2 MeV
f_B	λ_B	m_{B_d}	$m_b(m_b)$	τ_{B^+}	τ_{B^0}
200 MeV	(350 ± 150) MeV	5.279 GeV	4.2 ± 0.2 GeV	1.671ps	1.536ps
F_{K^*}	f_{K^*}	$f_{K^*}^\perp$	m_{K^*}	$\alpha_1^{K^*}$	$\alpha_2^{K^*}$
0.25 ± 0.06	230 MeV	185 MeV	894 MeV	0.2	0.04
F_ρ	f_ρ	f_ρ^\perp	m_ρ	α_1^ρ	α_2^ρ
0.29 ± 0.04	200 MeV	160 MeV	770 MeV	0	0.2

From Eqs.(11) and (14), the decay amplitude and branching ratio for $B \rightarrow K^* \gamma$ decay can be written as

$$A(\overline{B} \rightarrow K^* \gamma) = \frac{G_F}{\sqrt{2}} R_{K^*} \langle K^* \gamma | Q_7 | \overline{B} \rangle, \quad (31)$$

$$\mathcal{B}(\overline{B} \rightarrow K^* \gamma) = \tau_B \frac{G_F^2 \alpha m_B^3 m_b^2}{32\pi^4} \left(1 - \frac{m_{K^*}^2}{m_B^2}\right)^3 |R_{K^*}|^2 |F_{K^*}|^2, \quad (32)$$

with

$$R_{K^*} = V_{us}^* V_{ub} [a_7^u(K^* \gamma) + a_{ann}^u(K^* \gamma)] + V_{cs}^* V_{cb} [a_7^c(K^* \gamma) + a_{ann}^c(K^* \gamma)]. \quad (33)$$

The CP asymmetry of $B \rightarrow K^* \gamma$ can also be defined as [16]

$$\mathcal{A}_{CP}(K^* \gamma) = \frac{\Gamma(B \rightarrow K^* \gamma) - \Gamma(\overline{B} \rightarrow \overline{K}^* \gamma)}{\Gamma(B \rightarrow K^* \gamma) + \Gamma(\overline{B} \rightarrow \overline{K}^* \gamma)} \quad (34)$$

Another physical observable for $B \rightarrow V \gamma$ decay is the isospin symmetry breaking in the $K^{*\pm} - \overline{K}^{*0}$ or $\rho^\pm - \rho^0$ system. Since the branching ratios of both $B^- \rightarrow K^{*-} \gamma$ and $\overline{B}^0 \rightarrow \overline{K}^{*0} \gamma$ decays have been measured, the study of the isospin breaking in $B \rightarrow V \gamma$ decays becomes very interesting now [17, 20]. Following Ref. [17], the breaking of isospin symmetry in the $K^{*-} - \overline{K}^{*0}$ system can be defined as

$$\Delta_{0-}(K^* \gamma) \equiv \frac{\eta_\tau \mathcal{B}(B \rightarrow \overline{K}^{*0} \gamma) - \mathcal{B}(B \rightarrow K^{*-} \gamma)}{\eta_\tau \mathcal{B}(B \rightarrow \overline{K}^{*0} \gamma) + \mathcal{B}(B \rightarrow K^{*-} \gamma)}. \quad (35)$$

where $\eta_\tau = \tau_{B^+}/\tau_{B^0}$, and the CP-averaged branching ratios are understood.

By using the world averages as given in Eq. (2) and the ratio $\tau_{B^+}/\tau_{B^0} = 1.086 \pm 0.017$ [32], we find numerically that

$$\Delta_{0-}(K^*\gamma)^{exp} = (3.9 \pm 4.2)\%, \quad (36)$$

where the errors from the two measured branching ratios and the ratio τ_{B^+}/τ_{B^0} have been added in quadrature. The measured value of isospin symmetry breaking is indeed small as expected previously. Any new physics contribution producing large isospin breaking for $B \rightarrow K^*\gamma$ decays will be strongly constrained by this measurement.

A. Branching ratios and CP asymmetries

By using the formulas as given in Eqs.(13) and the central values of input parameters in Table I, the NLO SM predictions for branching ratio $\mathcal{B}(B \rightarrow K^*\gamma)$ are

$$\begin{aligned} \mathcal{B}(B \rightarrow \bar{K}^{*0}\gamma)^{SM} &= [3.36_{-1.30}^{+1.62}(F_{K^*})_{-0.60}^{+0.62}(\mu)_{-0.09}^{+0.23}(\lambda_B) \pm 0.20(m_c)] \times 10^{-5} \\ &= (3.36_{-1.45}^{+1.76}) \times 10^{-5}, \end{aligned} \quad (37)$$

$$\begin{aligned} \mathcal{B}(B \rightarrow K^{*-}\gamma)^{SM} &= [3.34_{-1.32}^{+1.66}(F_{K^*})_{-0.47}^{+0.28}(\mu)_{-0.12}^{+0.33}(\lambda_B) \pm 0.20(m_c)] \times 10^{-5} \\ &= (3.34_{-1.42}^{+1.72}) \times 10^{-5}, \end{aligned} \quad (38)$$

where the errors from the uncertainties of the input parameters have been added in quadrature, the largest theoretical error comes from the uncertainty of the form factor F_{K^*} : $F_{K^*} = 0.25 \pm 0.06$. By comparing these theoretical predictions with the measured values as given in Eq. (2), we can find that the central values are smaller than the world average, but they are in good agreement within one standard deviation.

According to previous studies in Ref. [23, 24], we got to know that the charged Higgs penguins can provide a significant contribution to the dominant Wilson coefficient $C_7(\mu)$. After taking into account the constraints from the data of $B \rightarrow X_s\gamma$, a charged Higgs boson with a mass Of 300 – 500 GeV is still allowed, as illustrated in Fig. 1. We now calculate the branching ratios and CP-violating asymmetries for the $B \rightarrow K^*\gamma$ in the T2HDM.

Using the input parameters as given in Table I, the theoretical predictions in the T2HDM are:

$$\begin{aligned} \mathcal{B}(B \rightarrow \bar{K}^{*0}\gamma)^{T2HDM} &= [3.85_{-1.49}^{+1.86}(F_{K^*})_{-0.34}^{+0.15}(\mu)_{-0.10}^{+0.26}(\lambda_B)_{-0.20}^{+0.21}(m_c)] \times 10^{-5} \\ &= (3.85_{-1.54}^{+1.90}) \times 10^{-5}, \end{aligned} \quad (39)$$

$$\begin{aligned} \mathcal{B}(B \rightarrow K^{*-}\gamma)^{T2HDM} &= [3.77_{-1.52}^{+1.92}(F_{K^*})_{-0.20}^{-0.11}(\mu)_{-0.14}^{+0.35}(\lambda_B) \pm 0.21(m_c)] \times 10^{-5} \\ &= (3.77_{-1.55}^{+1.97}) \times 10^{-5}, \end{aligned} \quad (40)$$

for $M_H = 400$ GeV, $\xi = 1$ and $\tan\beta = 30$.

Fig. 2 shows the M_H dependence of the branching ratio of $B \rightarrow K^{*-}\gamma$ decay in the SM and T2HDM for $\tan\beta = 10$ (solid curve), 30 (dashed curve) and 50 (dots curve), respectively. Three horizontal dots lines shows the central value and the 1σ lower and upper bounds of the SM prediction: $\mathcal{B}(B \rightarrow \bar{K}^{*0}\gamma) = (3.36_{-1.45}^{+1.76}) \times 10^{-5}$. The shaded

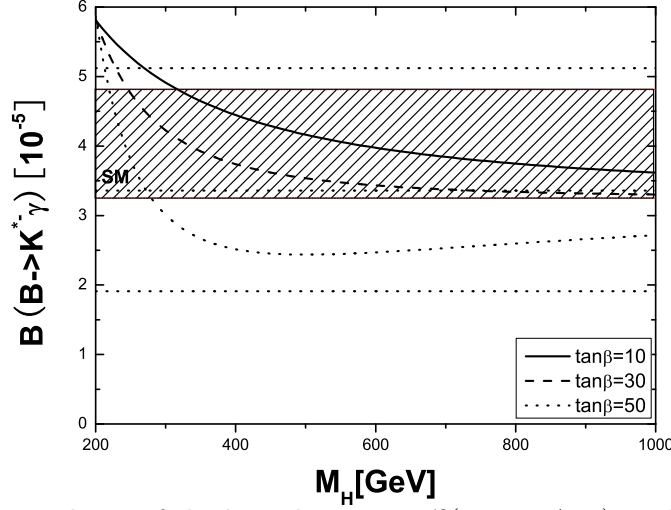


FIG. 2: The M_H dependence of the branching ratio $\mathcal{B}(B \rightarrow K^{*-}\gamma)$ in the T2HDM for $\tan\beta = 10, 30, 50$, respectively. More details see the text.

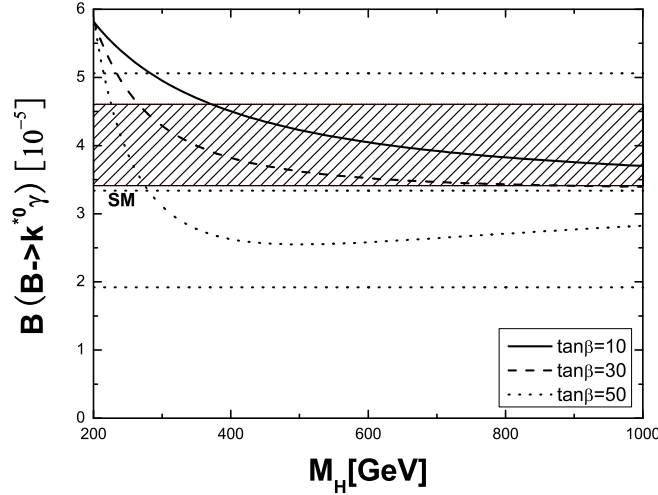


FIG. 3: The same as Fig.2, but for $B \rightarrow \bar{K}^{*0}\gamma$ decay.

band shows the region allowed by the data at 3σ level: $3.25 \times 10^{-5} \leq \mathcal{B}(B \rightarrow K^{*-}\gamma) \leq 4.81 \times 10^{-5}$.

Fig. 3 shows the M_H dependence of the branching ratio $B \rightarrow \bar{K}^{*0}\gamma$ in the SM and T2HDM for $\tan\beta = 10, 30, 50$, respectively. Three horizontal dots lines shows the central value and the 1σ lower and upper bounds of the SM prediction: $\mathcal{B}(B \rightarrow \bar{K}^{*0}\gamma) = (3.34^{+1.72}_{-1.42}) \times 10^{-5}$. The shaded band shows the region allowed by the data at 3σ level: $3.41 \times 10^{-5} \leq \mathcal{B}(B \rightarrow \bar{K}^{*0}\gamma) \leq 4.61 \times 10^{-5}$. Other curves have the same meaning as in Fig. 2.

Fig. 4 shows explicitly the $\tan\beta$ dependence of the branching ratio $B \rightarrow K^{*-}\gamma$ in the T2HDM for $M_H = 300, 500, 700$ GeV, respectively. The solid, dashed and dots curve shows the central value of the T2HDM prediction for $M_H = 300, 500$ and 700 GeV, respectively. Other curves in this figure have the same meaning as the corresponding curves in Fig. 2. For $B \rightarrow \bar{K}^{*0}\gamma$ decay channel, we found a very similar $\tan\beta$ dependence.

One can see from Figs.(2-4) that a light charged-Higgs boson with a mass less than 200

GeV is excluded by the data of $\mathcal{B}(B \rightarrow K^{*0,*-}\gamma)$, while a charged-Higgs boson with a mass larger than 300 GeV in the T2HDM is still allowed by the same data. This lower bound is well consistent with the one obtained from the data of the inclusive decay $B \rightarrow X_s\gamma$.

In Fig. 5, we show the θ dependence of the branching ratio $\mathcal{B}(B \rightarrow K^{*-}\gamma)$ in the T2HDM for $\tan\beta = 30$, $|\xi| = 1$, and $M_H = 300$ (solid curve), 500 (dashed curve) and 700 GeV (dotted curve), respectively.

For the exclusive $B \rightarrow K^*\gamma$ decay, the theoretical prediction for the CP-violating asymmetry \mathcal{A}_{CP} as defined in Eq. (34) is very small:

$$|\mathcal{A}_{CP}(B \rightarrow K^*\gamma)| < 1\% \quad (41)$$

in both the SM and the T2HDM considered here.

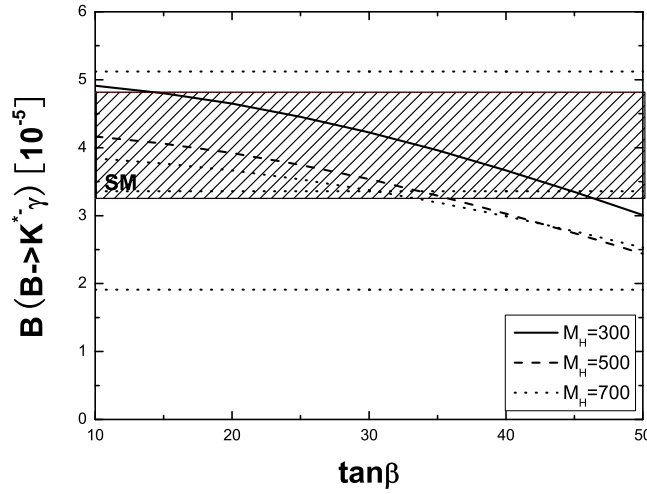


FIG. 4: The $\tan\beta$ dependence of the branching ratio $\mathcal{B}(B \rightarrow K^{*-}\gamma)$ in the T2HDM. The solid, dashed and dots curve shows the central value of the T2HDM prediction for $M_H = 300, 500, 700$ GeV, respectively.

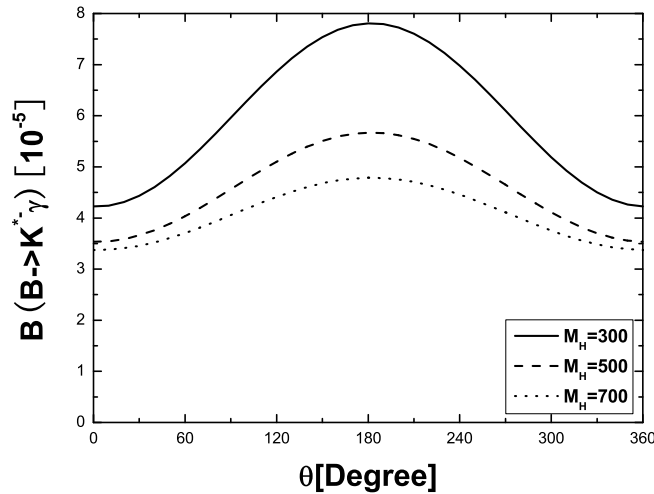


FIG. 5: The θ dependence of the branching ratio $\mathcal{B}(B \rightarrow K^{*-}\gamma)$ in the T2HDM. For details see the text.

B. Isospin Symmetry

In last subsection, one can see that it is the uncertainty of the form factor F_{K^*} which produces the dominant error for the theoretical predictions of the branching ratios, but such strong dependence on the form factor F_{K^*} will be largely canceled in the ratio for the isospin symmetry breaking of $B \rightarrow K^* \gamma$ system. From Eqs.(12,14), the isospin symmetry breaking $\Delta_{0-}(K^* \gamma)$ as defined in Eq. (35) can also be written as

$$\Delta_{0-}(K^* \gamma) = \frac{|R_{\overline{K}^{*0}}|^2 - |R_{K^{*-}}|^2}{|R_{\overline{K}^{*0}}|^2 + |R_{K^{*-}}|^2} \quad (42)$$

where the function R_{K^*} have been defined in Eq. (33).

In the SM, it is easy to find the numerical result for $\Delta_{0-}(K^* \gamma)$,

$$\begin{aligned} \Delta_{0-}(K^* \gamma)^{\text{SM}} &= [5.8_{-2.1}^{+4.1}(\mu)_{-1.0}^{+1.7}(F_{K^*})_{-1.3}^{+0.6}(\lambda_B)_{-0.1}^{+0.2}(m_c)] \times 10^{-2} \\ &= (5.8_{-2.7}^{+4.5}) \times 10^{-2}, \end{aligned} \quad (43)$$

where individual errors have been added in quadrature, and the remaining F_{K^*} dependence comes from the annihilation contributions which also have a relatively weak F_{K^*} dependence. The large theoretical error is dominated by the uncertainty of the low energy scale $m_b/2 \leq \mu \leq 2m_b$. The SM prediction are well consistent with the measured value of $\Delta_{0-}^{\text{exp}}(K^* \gamma) = (3.9 \pm 4.2)\%$.

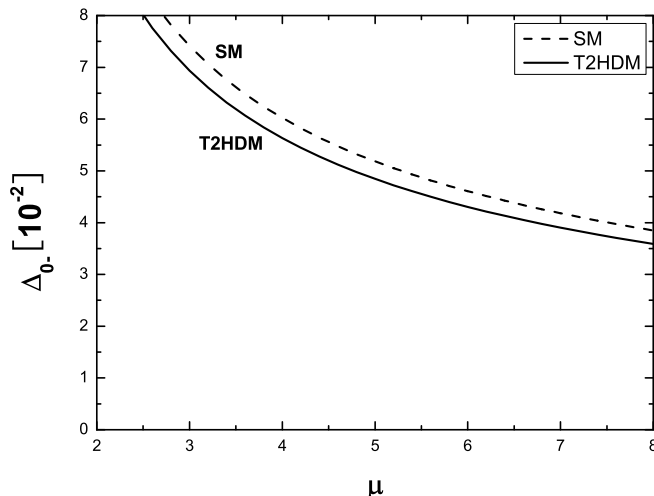


FIG. 6: The μ dependence of the isospin symmetry breaking $\Delta_{0-}(K^* \gamma)$ in the SM and T2HDM's. For details see the text.

In the top-quark two-Higgs-doublet model, and assuming $\xi = 1$, $\tan \beta = 30$ and $M_H = 400$ GeV, we find numerically that

$$\begin{aligned} \Delta_{0-}(K^* \gamma)^{\text{T2HDM}} &= [5.5_{-2.0}^{+3.8}(\mu)_{-1.0}^{+1.5}(F_{K^*})_{-1.1}^{+0.5}(\lambda_B) \pm 0.3(m_c)] \times 10^{-2} \\ &= (5.5_{-2.5}^{+4.1}) \times 10^{-2} \end{aligned} \quad (44)$$

where the individual errors have been added in quadrature, the dominant error comes from the uncertainty of the energy scale μ .

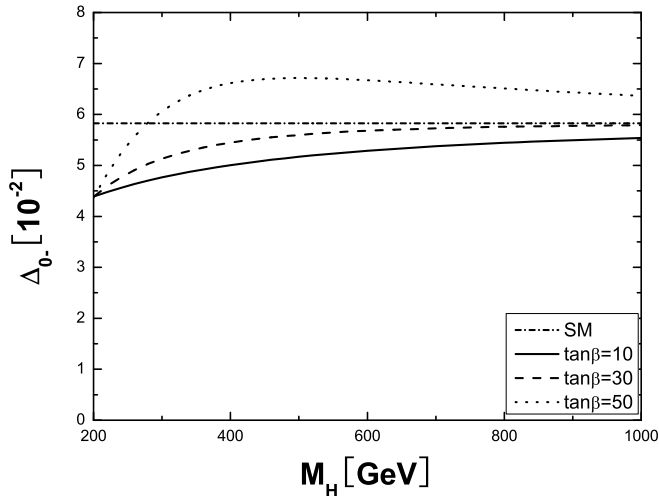


FIG. 7: The M_H dependence of the isospin symmetry breaking $\Delta_{0-}(K^*\gamma)$ in the SM and the T2HDM. For details see the text.

In Fig. 6, we show the μ dependence of the isospin symmetry breaking $\Delta_{0-}(K^*\gamma)$ in the SM and the T2HDM for $\xi = 1$, $\tan\beta = 30$ and $M_H = 400$ GeV. The dashed and solid curve shows the central value of the SM and T2HDM prediction, respectively. One can see from this figure that the new physics effects on the isospin symmetry breaking is very small. The reason is that the new physics contributions to the related decays are largely canceled in the ratio.

Of course, the isospin symmetry breaking in the T2HDM also have a moderate dependence on the values of M_H , $\tan\beta$ and ξ . Fig. 7 shows the M_H and $\tan\beta$ dependence of the isospin symmetry breaking $\Delta_{0-}(K^*\gamma)$ in the T2HDM's for $\xi = 1$. The solid, dashed and dots curve shows the T2HDM predictions for $\tan\beta = 10, 30$ and 50 , respectively. The dot-dash line shows the SM prediction. The whole region of Fig. 6 and 7 is allowed by the data: $\Delta_{0-}(K^*\gamma)^{exp} = (3.9 \pm 4.2) \times 10^{-2}$.

IV. $B \rightarrow \rho\gamma$ DECAY

When compared with $B \rightarrow K^*\gamma$ decay, the $B \rightarrow \rho\gamma$ decay mode is particularly interesting in search for new physics beyond the SM. Firstly, its branching ratio will be suppressed with respect to $B \rightarrow K^*\gamma$ by roughly a factor of $|V_{td}/V_{ts}|^2 \approx 4 \times 10^{-2}$. In contrast to the $B \rightarrow K^*\gamma$ decay, the CP-violating asymmetry for $B \rightarrow \rho\gamma$ decay is generally at 10% level and may be observed in B factory experiments.

A. Branching ratios and CP asymmetries

From Eq. (14), the branching ratios of $B \rightarrow \rho\gamma$ decays can be written as

$$\mathcal{B}(B \rightarrow \rho\gamma) = \tau_B \frac{G_F^2 \alpha m_B^3 m_b^2}{32\pi^4} \left(1 - \frac{m_\rho^2}{m_B^2}\right)^3 |R_\rho|^2 c_\rho^2 |F_\rho|^2, \quad (45)$$

with

$$R_\rho = V_{ud}^* V_{ub} [a_7^u(\rho\gamma) + a_{ann}^u(\rho\gamma)] + V_{cd}^* V_{cb} [a_7^c(\rho\gamma) + a_{ann}^c(\rho\gamma)]. \quad (46)$$

Using the input parameters as given in Table I, we find the SM predictions for the branching ratios and CP-violating asymmetries of $B \rightarrow \rho\gamma$ decays

$$\begin{aligned} \mathcal{B}(\overline{B}^0 \rightarrow \rho^0\gamma)^{\text{SM}} &= [0.77_{-0.18}^{+0.21}(F_\rho)_{-0.12}^{+0.09}(\mu_b)_{-0.02}^{+0.07}(\lambda_B)_{-0.15}^{+0.19}(\gamma)] \times 10^{-6} \\ &= (0.77_{-0.30}^{+0.35}) \times 10^{-6}, \end{aligned} \quad (47)$$

$$\begin{aligned} \mathcal{B}(B^- \rightarrow \rho^-\gamma)^{\text{SM}} &= [1.66 \pm 0.4(F_\rho)_{-0.11}^{+0.07}(\mu_b) \pm 0.3(\lambda_B)_{-0.16}^{+0.20}(\gamma)] \times 10^{-6} \\ &= (1.66 \pm 0.58) \times 10^{-6}, \end{aligned} \quad (48)$$

$$\begin{aligned} \mathcal{A}_{CP}(\rho^0\gamma)^{\text{SM}} &= [8.3_{-1.8}^{+3.8}(\mu_b)_{-1.6}^{+1.5}(R_b\&\gamma)_{-1.6}^{+0.8}(\lambda_B)_{-1.1}^{+0.9}(m_c)] \times 10^{-2} \\ &= (8.3_{-3.2}^{+4.3}) \times 10^{-2}, \end{aligned} \quad (49)$$

$$\begin{aligned} \mathcal{A}_{CP}(\rho^\pm\gamma)^{\text{SM}} &= [10.3_{-2.5}^{+5.4}(\mu_b)_{-2.0}^{+1.8}(R_b\&\gamma) \pm 0.8(m_c) \pm 0.1(\lambda_B)] \times 10^{-2} \\ &= (10.3_{-3.5}^{+5.8}) \times 10^{-2}, \end{aligned} \quad (50)$$

where the individual errors coming from uncertainties of F_ρ , μ_b , λ_B , m_c , R_b and γ have been taken into account and added in quadrature. As expected, the dominant error is induced by the uncertainty of the form factor F_ρ for the branching ratios, and by the uncertainty of the scale μ_b and the parameter R_b and γ for the CP-violating asymmetries.

For $M_H = 400$ GeV, $\tan\beta = 30$ and $\xi = 1$, the theoretical predictions for the branching ratios and CP-violating asymmetries of $B \rightarrow \rho\gamma$ decays in the T2HDM are as follows

$$\mathcal{B}(\rho^0\gamma)^{\text{NP}} = (0.88_{-0.34}^{+0.37}) \times 10^{-6}, \quad (51)$$

$$\mathcal{B}(\rho^-\gamma)^{\text{NP}} = (1.86_{0.63}^{+0.74}) \times 10^{-6}, \quad (52)$$

$$\mathcal{A}_{CP}(\rho^0\gamma)^{\text{NP}} = (7.8_{-2.7}^{+3.9}) \times 10^{-2}, \quad (53)$$

$$\mathcal{A}_{CP}(\rho^\pm\gamma)^{\text{NP}} = (11.1_{-3.7}^{+6.0}) \times 10^{-2}, \quad (54)$$

where the individual errors coming from uncertainties of F_ρ , μ_b , λ_B , m_c , R_b and γ have been taken into account and added in quadrature.

In Fig. 8, we show the M_H dependence of the branching ratio $\mathcal{B}(B \rightarrow \rho^0\gamma)$ in the T2HDM for $\xi = 1$, $\tan\beta = 10$ (solid curve), 30 (dashed curve) and 50 GeV (dotted curve), respectively. The central value and the error of the SM prediction as given in Eq.(26) are also shown by three horizontal dot-dash lines. Fig. 9 shows the M_H dependence of the branching ratio as in Fig. 8 but for $B^- \rightarrow \rho^-\gamma$ decay.

In the T2HDM, the CP-violating asymmetry has only a weak dependence on the value of M_H : $6.3\% \leq \mathcal{A}_{CP}(B \rightarrow \rho^0\gamma) \leq 8.3\%$ and $7.7\% \leq \mathcal{A}_{CP}(B \rightarrow \rho^\pm\gamma) \leq 11.1\%$ for $300\text{GeV} \leq M_H \leq 700$ GeV. But it has a strong dependence on the angle θ as expected. Fig. 10 shows the θ dependence of the CP-violating asymmetry for $B \rightarrow \rho^0\gamma$ (dashed curve) and $\rho^\pm\gamma$ decay (solid curve), assuming $\tan\beta = 30$, $|\xi| = 1$ and $M_H = 400$ GeV. Fig. 11 shows the CKM angle γ dependence of the CP-violating asymmetry for $B \rightarrow \rho^0\gamma$ (dashed curve) and $\rho^\pm\gamma$ decay (solid curve), assuming $\tan\beta = 30$, $\xi = 1$ and $M_H = 400$ GeV. The SM predictions are also shown by dot-dash ($\rho^0\gamma$ channel) and dotted curve ($\rho^\pm\gamma$ channel), respectively.

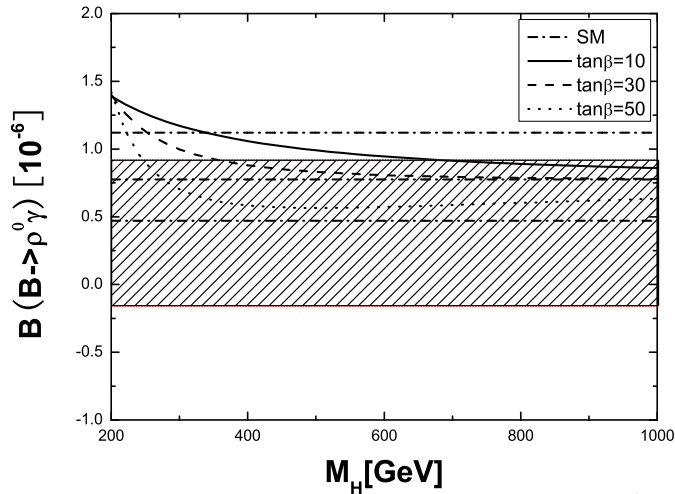


FIG. 8: Plots of the M_H dependence of the branching ratio $\mathcal{B}(B \rightarrow \rho^0 \gamma)$ in the SM (short-dash curves) and T2HDM (solid, dashed and dots curve for $\tan\beta = 10, 30, 50$, respectively). The shaded band shows the data at 3σ level.

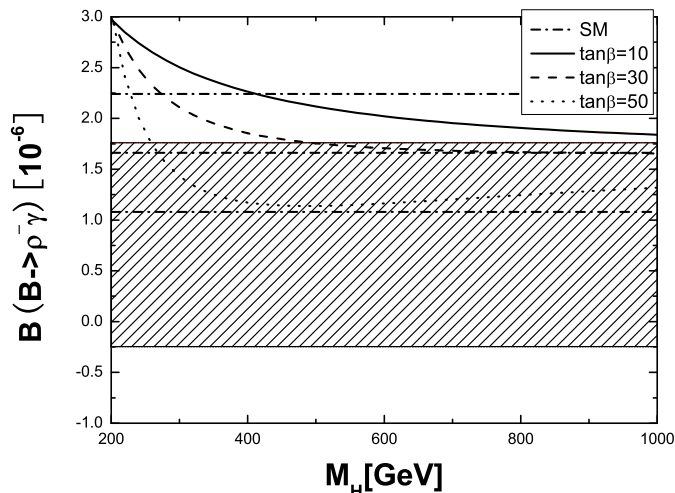


FIG. 9: The same as Fig. 8 but for $B \rightarrow \rho^- \gamma$ decay.

By comparing the above theoretical predictions in the SM and T2HDM with the measured values of branching ratios as given in Eqs.(3) and (4), we find that

- (i) The central values of the theoretical predictions for the branching ratios are generally larger than the measured values, but still consistent with them within two standard deviation, as shown in Figs. 8 and 9. Since the theoretical predictions for the branching ratios are proportional to the value of the form factor F_ρ , the current data clearly prefer a smaller F_ρ , just like the case of $B \rightarrow K^* \gamma$ decays.
- (ii) The new physics contributions tend to increase the branching ratios for light charged-Higgs boson, but such enhancement become smaller rapidly when the charged-Higgs boson becoming heavy, as illustrated in Figs. 8 and 9. For a charged-Higgs boson with a mass around 400 GeV, the theoretical predictions in the T2HDM become compatible with the data and the SM predictions.
- (iii) In the T2HDM, the CP-violating asymmetry has a strong θ dependence for

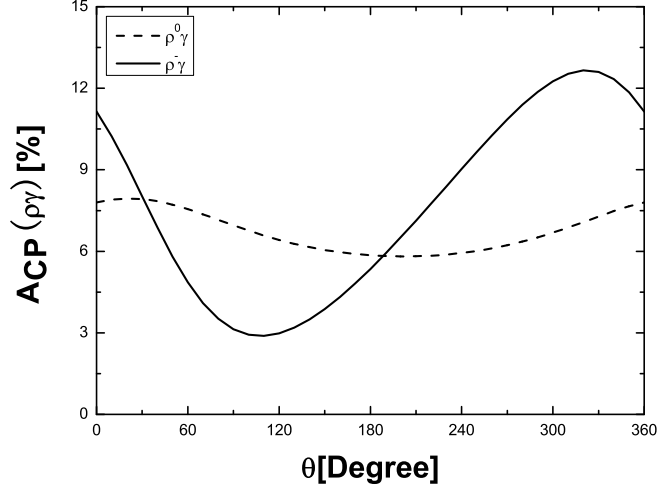


FIG. 10: Plots of θ dependence of the CP-violating asymmetries for $B \rightarrow \rho^0\gamma$ (dashed curve) and $B^\pm \rightarrow \rho^\pm\gamma$ (solid curve) decay in the T2HDM, assuming $M_H = 400$ GeV, $\tan\beta = 30$ and $|\xi| = 1$.

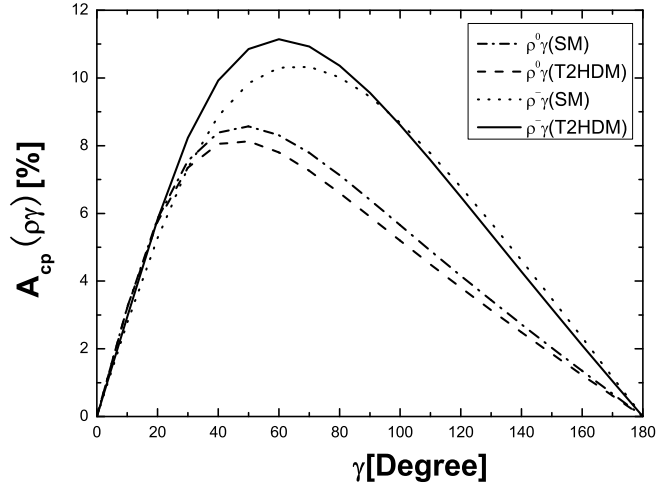


FIG. 11: Plots of the CKM angle γ dependence of the CP asymmetries for $B \rightarrow \rho\gamma$ decays in the SM and T2HDM, assuming $M_H = 400$ GeV, $\tan\beta = 30$ and $\xi = 1$.

$$B^\pm \rightarrow \rho^\pm\gamma \text{ decay: } 2.9\% \leq \mathcal{A}_{CP}(B \rightarrow \rho^\pm\gamma) \leq 12.7\%.$$

(iv) One can see from the numerical results that a charged-Higgs boson with a mass of 300 – 500 GeV is still allowed by the data of $B \rightarrow \rho\gamma$.

B. Isospin and U-spin symmetries

In Refs. [15, 16], the isospin symmetry breaking of $B \rightarrow \rho\gamma$ decays has been defined as the form of

$$\Delta(\rho\gamma) = \frac{1}{2} \left[\frac{\Gamma(B^+ \rightarrow \rho^+\gamma)}{2\Gamma(B^0 \rightarrow \rho^0\gamma)} + \frac{\Gamma(B^- \rightarrow \rho^-\gamma)}{2\Gamma(\bar{B}^0 \rightarrow \rho^0\gamma)} - 2 \right]. \quad (55)$$

Using the central values of input parameters as listed in Table I and assuming $\tan\beta = 30$, $M_H = 400$ GeV, we find numerically

$$\Delta(\rho\gamma) = \begin{cases} (0.7_{-11.5}^{+19.0}) \times 10^{-2}, & \text{in SM,} \\ (0.4_{-10.2}^{+17.6}) \times 10^{-2}, & \text{in T2HDM,} \end{cases} \quad (56)$$

where the errors coming from uncertainties of input parameters have been added in quadrature. The uncertainty of the CKM angle γ and the parameter λ_B dominate the total theoretical error. Although the central value of the isospin breaking $\Delta(\rho\gamma)$ is very small, but it can be as large as 10% – 20% in the parameter space considered. The new physics correction on $\Delta(\rho\gamma)$ is too small to be separated experimentally.

Under the approximation $\Gamma(B^+ \rightarrow \rho^+\gamma) = \Gamma(B^- \rightarrow \rho^-\gamma)$, and $\Gamma(B^0 \rightarrow \rho^0\gamma) = \Gamma(\overline{B}^0 \rightarrow \rho^0\gamma)$, Eq. (55) can be rewritten as

$$\Delta(\rho\gamma)^{exp} = \frac{1}{2} \left[\frac{\tau_{B^0} \mathcal{B}(B \rightarrow \rho^\pm\gamma)^{exp}}{\tau_{B^+} \mathcal{B}(B \rightarrow \rho^0\gamma)^{exp}} - 2 \right], \quad (57)$$

and we find numerically

$$\Delta(\rho\gamma)^{exp} = -0.18_{-0.38}^{+0.44} (\mathcal{B}(\rho^\pm\gamma))_{-0.26}^{+0.74} (\mathcal{B}(\rho^0\gamma)) = -0.18_{-0.46}^{+0.86} \quad (58)$$

by using the measured values of the branching ratios and lifetimes as given in Eq.(4) and in Ref. [32]. Although the central value of $\Delta(\rho\gamma)^{exp}$ is in the reasonable region, but its error is too large to compare meaningfully with the theoretical predictions.

In Fig.12, we show the angle γ dependence of the isospin symmetry breaking $\Delta(\rho\gamma)$ in the SM and the T2HDM for $\tan\beta = 30$, $\xi = 1$ and $M_H = 300$ (solid curve), 500 (dashed curve) and 700 GeV (dotted curve). It is easy to see from Fig.12 that

- (i) The isospin breaking in the SM and T2HDM's have the similar γ dependence;
- (ii) All theoretical predictions become almost identical and very small in magnitude for $\gamma \sim 60^\circ$, the value of γ preferred by the global fit. The smallness of $\Delta(\rho\gamma)$ is also consistent with the general expectation and other measurements;
- (iii) The theoretical predictions in the SM and T2HDM have the similar γ dependence, and have the same sign for small or large values of the CKM angle γ .

Another interesting observable for $B \rightarrow (K^*, \rho)\gamma$ decays is the U-spin symmetry, it has been studied in Refs.[15, 16, 35]. In the limit of U-spin symmetry, the quantity

$$\Delta U(K^*, \rho) \equiv \Delta\mathcal{B}(B \rightarrow K^*\gamma) + \Delta\mathcal{B}(B \rightarrow \rho\gamma) \equiv 0 \quad (59)$$

with

$$\Delta\mathcal{B}(B \rightarrow K^*\gamma) = \mathcal{B}(B^+ \rightarrow K^{*+}\gamma) - \mathcal{B}(B^- \rightarrow K^{*-}\gamma), \quad (60)$$

$$\Delta\mathcal{B}(B \rightarrow \rho\gamma) = \mathcal{B}(B^+ \rightarrow \rho^+\gamma) - \mathcal{B}(B^- \rightarrow \rho^-\gamma), \quad (61)$$

should be satisfied. Using the central values of input parameters, we find the SM predictions for $\Delta\mathcal{B}(B \rightarrow K^*\gamma)$ and $\Delta\mathcal{B}(B \rightarrow \rho\gamma)$

$$\Delta\mathcal{B}(B \rightarrow K^*\gamma) = -3.3 \times 10^{-7}, \quad \Delta\mathcal{B}(B \rightarrow \rho\gamma) = +3.8 \times 10^{-7}. \quad (62)$$

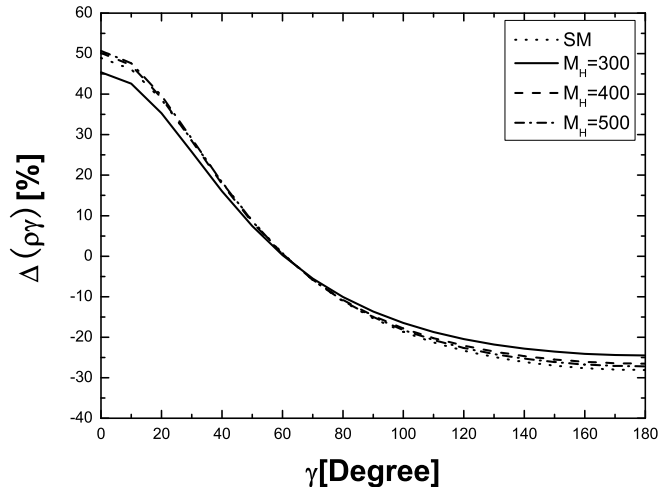


FIG. 12: The isospin breaking $\Delta(\rho\gamma)$ vs the CKM angle γ in the SM (dots curves) and T2HDM (solid curve).

Here we have chosen $\gamma = 60^\circ$ which maximizes the effects. The two parts have opposite sign and cancels to a large extent, leaving a small U-spin breaking

$$\Delta U(K^*, \rho) = 0.5 \times 10^{-7}. \quad (63)$$

in the SM, which is only about 8% of the branching ratio $\mathcal{B}(B \rightarrow \rho^0\gamma)$. In the T2HDM, we find the numerical result

$$\Delta U(K^*, \rho) = 1.1 \times 10^{-7}, \quad (64)$$

for $\tan\beta = 30$, $M_H = 400$ GeV and $\gamma = 60^\circ$. The new physics contribution in the conventional T2HDM has little effect on the size of U-spin symmetry breaking.

V. CONCLUSIONS

By employing the QCD factorization approach for the exclusive $B \rightarrow V\gamma$ decays as proposed in Refs.[13, 14, 15], we calculated the new physics contributions to the branching ratios, CP asymmetries, isospin symmetry breaking and U-spin symmetry breaking of the exclusive radiative decays $B \rightarrow K^*\gamma$ and $B \rightarrow \rho\gamma$, induced by the charged Higgs penguin diagrams appeared in the top-quark two-Higgs-doublet model [22, 23, 24]. The new physics contributions are included through their corrections to the Wilson coefficients $C_7(M_W)$ and $C_8(M_W)$ at the matching scale M_W .

In section II, we describe briefly the basic structures of the T2HDM, give a brief review about the calculation of $B \rightarrow V\gamma$ ($V = K^*, \rho$) at NLO in QCD factorization approach and present the needed analytical formulas.

In section III and IV, we calculated the new physics contributions to the physical observable of $B \rightarrow K^*\gamma$ and $B \rightarrow \rho\gamma$ decays in the T2HDM, compared the theoretical predictions with those currently available experimental measurements, and we found that:

- (i) In the T2HDM, a light charged-Higgs boson with a mass less than 200 GeV is clearly excluded by the date of $B \rightarrow V\gamma$ decay, but a charged-Higgs boson with a

mass larger than 300 GeV are always allowed by the same set of data. Such lower limits on M_H are comparable with those obtained from the inclusive $B \rightarrow X_s \gamma$ decay.

(ii) In the SM and T2HDM, the theoretical predictions for CP asymmetry of $B \rightarrow K^* \gamma$ is always less than 1% in size, but CP asymmetry of $B \rightarrow \rho \gamma$ can be as large as 10% in magnitude and have a strong dependence on the variations of the angle θ , the scale $\mu = \mathcal{O}(m_b)$ and the CKM angle γ .

(iii) The isospin symmetry breaking for $B \rightarrow V \gamma$ decays in the SM and T2HDM considered here are generally small in size: around 6% for $B \rightarrow K^* \gamma$ decay (well consistent with the data), and in the range of $[-0.11, 0.20]$ for $B \rightarrow \rho \gamma$ when the effects of theoretical uncertainties of input parameters are also taken into account.

(iv) The U-spin symmetry breaking $\Delta U(K^*, \rho)$ in the SM and T2HDM's considered here is generally small in size, only about 8% of the branching ratio $\mathcal{B}(B \rightarrow \rho^0 \gamma)$.

Acknowledgments

We are very grateful to Li-bo Guo for helpful discussions. This work is partially supported by the National Natural Science Foundation of China under Grant No.10275035, 10575052 and by the Specialized Research Fund for the doctoral Program of higher education (SRFDP) under Grant No. 20050319008.

APPENDIX A: WILSON COEFFICIENTS

At the low energy scale $\mu = \mathcal{O}(m_b)$, the leading order Wilson coefficients are

$$C_{j,\text{SM}}^0(\mu) = \sum_{i=1}^8 k_{ji} \eta^{a_i}, \quad \text{for } j = 1, \dots, 6, \quad (\text{A1})$$

$$C_{7,\text{SM}}^0(\mu) = \eta^{\frac{16}{23}} C_{7,\text{SM}}^0(M_W) + \frac{8}{3} (\eta^{\frac{14}{23}} - \eta^{\frac{16}{23}}) C_{8,\text{SM}}^0(M_W) + \sum_{i=1}^8 h_i \eta^{a_i}, \quad (\text{A2})$$

$$C_{8,\text{SM}}^0(\mu) = C_{8,\text{SM}}^0(M_W) \eta^{\frac{14}{23}} + \sum_{i=1}^8 \tilde{h}_i \eta^{a_i} \quad (\text{A3})$$

in the standard basis, while

$$Z_{j,\text{SM}}^0(\mu) = \sum_{i=1}^8 h_{ji} \eta^{a_i}, \quad \text{for } j = 1 \dots 6, \quad (\text{A4})$$

$$Z_{7,\text{SM}}^0(\mu) = C_{7,\text{SM}}^0(\mu), \quad (\text{A5})$$

$$Z_{8,\text{SM}}^0(\mu) = C_{8,\text{SM}}^0(\mu) \quad (\text{A6})$$

in the CMM basis. Here $\eta = \alpha_s(M_W)/\alpha_s(\mu_b)$, and the expressions of the Wilson coefficients $C_{7,\text{SM}}^0(M_W)$ and $C_{8,\text{SM}}^0(M_W)$, the “magic numbers” a_i , k_{ji} , h_{ji} , h_i and \tilde{h}_i can be found in Ref. [1].

The NLO Wilson coefficient $C_7(\mu_b)$ at scale $\mu_b = \mathcal{O}(m_b)$ can be written as

$$C_{7,\text{SM}}(\mu) = C_{7,\text{SM}}^0(\mu) + \frac{\alpha_s(\mu)}{4\pi} C_{7,\text{SM}}^1(\mu) \quad (\text{A7})$$

with

$$\begin{aligned} C_{7,\text{SM}}^1(\mu) &= \eta^{\frac{39}{23}} C_{7,\text{SM}}^1(M_W) + \frac{8}{3} \left(\eta^{\frac{37}{23}} - \eta^{\frac{39}{23}} \right) C_{8,\text{SM}}^1(M_W) \\ &+ \left(\frac{297664}{14283} \eta^{\frac{16}{23}} - \frac{7164416}{357075} \eta^{\frac{14}{23}} + \frac{256868}{14283} \eta^{\frac{37}{23}} - \frac{6698884}{357075} \eta^{\frac{39}{23}} \right) C_{8,\text{SM}}^0(M_W) \\ &+ \frac{37208}{4761} \left(\eta^{\frac{39}{23}} - \eta^{\frac{16}{23}} \right) C_{7,\text{SM}}^0(M_W) + \sum_{i=1}^8 (e_i \eta E(x_t) + f_i + g_i \eta) \eta^{a_i}, \end{aligned} \quad (\text{A8})$$

where the function $E(x_t)$ and the ‘‘magic numbers’’ e_i , f_i and g_i can also be found in Ref. [1].

APPENDIX B: G_i AND H_i^V FUNCTIONS

In this Appendix, the explicit expressions or numerical values of all G_i and H_i^V functions appeared in Eq. (11) will be listed. For more details of these functions, one can see Ref. [16] and references therein.

$$G_1(z) = \frac{52}{81} \ln \frac{\mu}{m_b} + \frac{833}{972} - \frac{1}{4} [a(z) + b(z)] + \frac{10i\pi}{81}, \quad (\text{B1})$$

$$G_2(z) = -\frac{104}{27} \ln \frac{\mu}{m_b} - \frac{833}{162} + \frac{3}{2} [a(z) + b(z)] - \frac{20i\pi}{27}, \quad (\text{B2})$$

$$G_3 = \frac{44}{27} \ln \frac{\mu}{m_b} + \frac{598}{81} + \frac{2\pi}{\sqrt{3}} + \frac{8}{3} X_b - \frac{3}{4} a(1) + \frac{3}{2} b(1) + \frac{14i\pi}{27}, \quad (\text{B3})$$

$$G_4(z_c) = \frac{38}{81} \ln \frac{\mu}{m_b} + \frac{761}{972} - \frac{\pi}{3\sqrt{3}} - \frac{4}{9} X_b + \frac{1}{8} a(1) + \frac{5}{4} b(z_c) - \frac{37i\pi}{81} \quad (\text{B4})$$

$$G_5 = \frac{1568}{27} \ln \frac{\mu}{m_b} + \frac{14170}{81} + \frac{8\pi}{\sqrt{3}} + \frac{32}{3} X_b - 12a(1) + 24b(1) + \frac{224i\pi}{27}, \quad (\text{B5})$$

$$\begin{aligned} G_6(z_c) &= -\frac{1156}{81} \ln \frac{\mu}{m_b} + \frac{2855}{486} - \frac{4\pi}{3\sqrt{3}} - \frac{16}{9} X_b \\ &- \frac{5}{2} a(1) + 11b(1) + 9a(z_c) + 15b(z_c) - \frac{574i\pi}{81}, \end{aligned} \quad (\text{B6})$$

$$G_8 = \frac{8}{3} \ln \frac{\mu}{m_b} + \frac{11}{3} - \frac{2\pi^2}{9} + \frac{2i\pi}{3}, \quad (\text{B7})$$

$$(\text{B8})$$

where

$$X_b = \int_0^1 dx \int_0^1 dy \int_0^1 dv xy \ln[v + x(1-x)(1-v)(1-v+vy)] \approx -0.1684, \quad (\text{B9})$$

$$a(1) \simeq 4.0859 + \frac{4i\pi}{9}, \quad (\text{B10})$$

$$b(1) = \frac{320}{81} - \frac{4\pi}{3\sqrt{3}} + \frac{632\pi^2}{1215} - \frac{8}{45} \left[\frac{d^2 \ln \Gamma(x)}{dx^2} \right]_{x=\frac{1}{6}} + \frac{4i\pi}{81} \simeq 0.0316 + \frac{4i\pi}{81}, \quad (\text{B11})$$

$$a(z_u) = (-1.93 + 4.96i) \times 10^{-5}, \quad (\text{B12})$$

$$a(z_c) = 1.525 + 1.242i, \quad (\text{B13})$$

$$b(z_u) = (1.11 + 0.28i) \times 10^{-5}, \quad (\text{B14})$$

$$b(z_c) = -0.0195 + 0.1318i, \quad (\text{B15})$$

where $z_q = m_q^2/m_b^2$ and the masses m_q ($q = u, c, b$) as listed in Table I have been used to obtain the numerical results. The explicit analytical expressions for $a(z)$ and $b(z)$ can be found for example in Ref. [16].

For the H_i^V functions, we have

$$H_1^V(z_p) = -\frac{2\pi^2}{9} \frac{f_B f_V^\perp}{F_V m_B \lambda_B} \int_0^1 dv h(\bar{v}, z_p) \Phi_V^\perp(v), \quad (\text{B16})$$

$$H_2^V = 0 \quad (\text{B17})$$

$$H_3^V = -\frac{1}{2} [H_1^V(1) + H_1^V(0)], \quad (\text{B18})$$

$$H_4^V(z_c) = H_1^V(z_c) - \frac{1}{2} H_1^V(1), \quad (\text{B19})$$

$$H_5^V = 2H_1^V(1), \quad (\text{B20})$$

$$H_6^V(z_c) = -H_1^V(z_c) + \frac{1}{2} H_1^V(1) = -H_4^V(z_c), \quad (\text{B21})$$

$$H_8^V = +\frac{4\pi^2}{3} \frac{f_B f_V^\perp}{F_V m_B \lambda_B} (1 - \alpha_1^V + \alpha_2^V + \dots), \quad (\text{B22})$$

where the hard-scattering function $h(u, z)$ is given by

$$h(u, z) = \frac{4z}{u^2} \left\{ Li_2 \left[\frac{2}{1 - \sqrt{\frac{u-4z+i\varepsilon}{u}}} \right] + Li_2 \left[\frac{2}{1 + \sqrt{\frac{u-4z+i\varepsilon}{u}}} \right] \right\} - \frac{2}{u}, \quad (\text{B23})$$

where $Li_2[x]$ is the dilogarithmic function, and the function $h(u, z)$ is real for $u \leq 4z$ and develops an imaginary part for $u > 4z$. The light-cone wave function $\Phi_V^\perp(v)$ takes the form of

$$\Phi_V^\perp(v) = 6v(1-v) \left[1 + \alpha_1^V(\mu) C_1^{3/2}(2v-1) + \alpha_2^V(\mu) C_2^{3/2}(2v-1) + \dots \right] \quad (\text{B24})$$

where $C_1^{3/2}(x) = 3x$, $C_2^{3/2}(x) = \frac{3}{2}(5x^2 - 1)$.

-
- [1] G. Buchalla, A.J. Buras, and M.E. Lautenbacher, *Rev. Mod. Phys.* **68**, 1125 (1996).
- [2] T. Hurth, *Rev. Mod. Phys.* **75**, 1159(2003).
- [3] T. Hurth, talk presented at Beauty 2005, Perugia, Italy, 20 -24 June, 2005; S.W. Bosch, talk presented at CKM2005 Workshop, San Diego, USA, 15-18 March, 2005; C. Bobeth, talk presented at CKM2005 Workshop, San Diego, USA, 15-18 March, 2005.
- [4] Heavy Flavor Averaging Group, <http://www.slac.stanford.edu/xorg/hfag>.
- [5] A.L. Kagan and M. Neubert, *Eur. Phys. J. C* **7**, 5 (1999); A.J. Buras, A. Czarnecki, M. Misiak, and J. Urban, *Nucl. Phys. B* **611**, 488 (2001), **631**, 219 (2002).
- [6] M. Carena, D. Garcia, U. Nierste and C. E. Wagner, *Phys. Lett. B* **499**,141 (2001); G. Degrassi, P. Gambino and G. F. Giudice, *JHEP* **0012**, 009 (2000); G. D'Ambrosio, G. F. Giudice, G. Isidori and A. Strumia, *Nucl. Phys. B* **645**, 255 (2002).
- [7] F. Borzumati, C. Greub, T. Hurth and D. Wyler, *Phys. Rev. D* **62**, 075005 (2000); T. Be-smer, C. Greub and T. Hurth, *Nucl. Phys. B* **609**, 359 (2001).
- [8] S. Glashow and S. Weinberg, *Phys. Rev. D* **15**, 1958 (1977); J.F. Gunion, H.E. Haber, G. Kane, and S. Dawson, *The Higgs Hunter's Guide*, Addison Wesley, Redwood-City (1990), and references therein.
- [9] Z.J. Xiao and L.B. Guo, *Phys. Rev. D* **69**, 014002 (2004).
- [10] D. Mohapatra *et al.*, Belle Collab., *Phys. Rev. D* **72**, 011101(R) (2005); K. Abe *et al.*, Belle Collab., hep-ex/0506079.
- [11] N.G. Deshpande, P. Lo, J. Trampetic, G. Eilam, and P. Singer, *Phys. Rev. Lett.* **59**, 183 (1987).
- [12] C. Greub, H. Simma and D. Wyler, *Nucl. Phys. B* **434**, 39 (1995); H.H. Asatryan, H.M. Asatrian, and D. Wyler, *Phys. Lett. B* **470**, 223 (1999).
- [13] M. Beneke, T. Feldmann and D. Seidel, *Nucl. Phys. B* **612**, 25 (2001).
- [14] A. Ali and A.Y. Parkhomenko, *Eur. Phys. J. C* **23**, 89 (2002).
- [15] S.W. Bosch and G. Buchalla, *Nucl. Phys. B* **621**, 459 (2002).
- [16] S.W. Bosch, *Exclusive Radiative Decays of B Mesons in QCD Factorization*, PH.D thesis, hep-ph/0208203.
- [17] A.L. Kagan and M. Neubert, *Phys. Lett. B* **539**, 227 (2002).
- [18] H.-n. Li and G.L. Lin, *Phys. Rev. D* **60**, 054001 (1999).
- [19] C.D. Lü, M. Matsumori, A.I. Sanda and M.Z. Yang, *Phys. Rev. D* **72**, 094005 (2005).
- [20] A. Ali, T. Handoko, and D. London, *Phys. Rev. D* **63**, 014014 (2001); A.Arhib, C.K. Chua and W.S. Hou, *Eur. Phys. J. C* **21**, 567 (2001); A. Ali and E. Lunghi, *Eur. Phys. J. C* **26**, 195 (2002).
- [21] Z.J. Xiao and C. Zhuang, *Eur. Phys. J. C* **33**, 349 (2004).
- [22] A.Das and C.Kao, *Phys. Lett. B* **372**, 106 (1996).
- [23] K. Kiers, A. Soni, and G.H. Wu, *Phys. Rev. D* **59**, 096001 (1999); G.H. Wu and A. Soni, *Phys. Rev. D* **62**, 056005 (2000).
- [24] K. Kiers, A. Soni, and G.H. Wu, *Phys. Rev. D* **62**, 116004 (2000).
- [25] M. Kobayashi, T. Maskawa, *Prog. Theor. Phys.* **49**, 652 (1973).
- [26] K.G. Chetyrkin, M. Misiak, M. Munz, *Phys. Lett. B* **400**, 206(1997), **425**, 414(E) (1998).
- [27] A.J. Buras, M. Misiak, M. Münz, and S. Pokorski, *Nucl. Phys. B* **424**, 374 (1994).
- [28] T.P. Cheng and M. Sher, *Phys. Rev. D* **35**, 3484 (1987); M. Sher and Y. Yuan, *Phys. Rev.*

- D **44**, 1461 (1991); W.S. Hou, Phys. Lett. B **296**, 179 (1992); A. Antaramian, L.J. Hall, and A. Rasin, Phys. Rev. Lett. **69**, 1871 (1992); L.J. Hall and S. Winberg, Phys. Rev. D **48**, R979 (1993); D. Chang, W.S. Hou, and W.Y. Keung, Phys. Rev. D **48**, 217 (1993); Y.L. Wu and L. Wolfenstein, Phys. Rev. Lett. **73**, 1762 (1994); D. Atwood, L. Reina and A. Soni, Phys. Rev. Lett. **75**, 3800 (1995).
- [29] D. Atwood, L. Reina and A. Soni, Phys. Rev. D **55**, 3156 (1997); T.M. Aliev and E.O. Iltan, J. Phys. G **25**, 989 (1999); D.B. Chao, K. Heung, and W.Y. Keung, Phys. Rev. D **59**, 115006 (1999).
- [30] Z.J. Xiao, C.S. Li, and K.T. Chao, Phys. Lett. B **473**, 148 (2000); Z.J. Xiao, C.S. Li, and K.T. Chao, Phys. Rev. D **63**, 074005 (2001); J.J. Cao, Z.J. Xiao, and G.R. Lu, Phys. Rev. D **64**, 014012 (2001); D. Zhang, Z.J. Xiao, and C.S. Li, Phys. Rev. D **64**, 014014 (2001); Z.J. Xiao, K.T. Chao, and C.S. Li, Phys. Rev. D **65**, 114021 (2002).
- [31] F.M. Borzumati and C. Greub, Phys. Rev. D **58**, 074004 (1998); *ibid* **59**, 057501 (1999).
- [32] Particle Data Group, S. Eidelman *et al.*, Phys. Lett. B **592**, 1(2004).
- [33] P. Ball and V.M. Braun, Phys. Rev. D **58**, 094016 (1998).
- [34] D. Becirevic. talk given at the Ringberg Phenomenology Workshop on heavy flavors, Ringberg Castle, Tegernsee, Germany, May 2003.
- [35] M. Gronau and J.L. Rosner, Phys. Lett. B **500**, 247 (2001); M. Gronau, Phys. Lett. B **492**, 297 (2000); T. Hurth and T. Mannel, Phys. Lett. B **511**, 196 (2001); R. Fleischer, Phys. Lett. B **459**, 306 (1999).